



Contents lists available at [Egyptian Knowledge Bank](https://egyptianknowledgebank.com)  
**Advances in Environmental and Life  
 Sciences**

journal homepage: <https://aels.journals.ekb.eg>



## An eco-friendly resorcinol derivative as an inhibitor for pitting and microbial corrosion: Experimental and theoretical inspections

Medhat M Kamel<sup>a</sup>, Mostafa A A Mahmoud<sup>a,\*</sup>, Salah M Rashwan<sup>a</sup>, Sameh A Elmekawy<sup>b</sup>, Hoyida E Ibrahim<sup>a</sup>, Mohamed K Awad<sup>c</sup>

<sup>a</sup> Department of Chemistry, Faculty of Science, Suez Canal University, Ismailia 41522, Egypt.

<sup>b</sup> Department of Physics and Mathematics, Faculty of Engineering, Port Said University, Port Said, Egypt.

<sup>c</sup> Theoretical Applied Chemistry Unit (TACU), Chemistry Department, Faculty of Science, Tanta, Egypt.

### Abstract

This article describes the synthesis of 4, 6-dihydroxyisophthalohydrazide (DIH) and its characterization using <sup>1</sup>H-NMR spectroscopy and evaluate its inhibiting performance against the aggressive attack of HCl on low carbon steel (CS). Chemistry and electrochemistry tools were used to investigate the inhibitor's effectiveness. In line with the Langmuir adsorption model, the results showed that the DIH compound greatly reduces the disintegration rate of CS by the adsorption process. Tafel data and EIS results showed that, the compound has a mixed-type characteristic. Raising the DIH concentration from 50 to 300 ppm reduces the charge transfer ( $R_{ct}$ ) of CS from 48.6 to 351.3 ohm  $cm^2$  and decreasing the adsorbed double layer's capacitance from  $108 \times 10^{-6}$  to  $13 \times 10^{-6}$  F  $cm^{-2}$ , respectively. A dosage of 300 ppm is optimal for 86.2 % inhibition effectiveness. Calculations using Monte Carlo (MC) simulations showed that the synthesized compound adhered to the CS quite well. The SEM/AFM results confirmed the existence of a protective film on the CS specimen. The in-vitro data that appeared from the killing test by using Postgate B media against SRB bacteria revealed the ability of DIH compound to reduce the perforation of bacteria from  $10^6$  cells/ml to nil at dosage of 300 ppm. The molecular docking simulation confirmed the obtained results.

**Keywords:** Resorcinol derivative, Pitting Corrosion, Microbial Corrosion, Carbon steel, Molecular


### 1. Introduction

Corrosion inhibitors are required for various industrial operations to regulate the pace at which metallic structures corrode [1–3]. In addition, the inhibitors are extremely useful for industrial acidic applications involving carbon steel surfaces, like acid cleaning, pickling, etching, surface cleaning, and oxide layer removal [4–6]. Typically, effective organic inhibitors have O, S, or N atoms and function groups with electronegativity and electrons in

triple and conjugated double bonds, in their structure [7]. These compounds had a unique chemical composition that contained the elements carbon, hydrogen, oxygen, and nitrogen. In addition, have an inhibition effect on metal corrosion [8].

Corrosion of steel has been established by many studies [9–13]. Mixed inhibitor of CTAB (cetyltrimethylammonium) and (SDS) sodium dodecyl sulfate bromide was utilized in 3.5% NaCl solution as a corrosion inhibitor [9]. The inhibitor declines both the rate of cathodic and anodic reactions. Also, another study used sodium gluconate and CTAB in 3.0% NaCl solution on galvanized steel, this resulting in a reduction in the cathodic

\*Corresponding author.

Email address: [maam403.ms@gmail.com](mailto:maam403.ms@gmail.com) (Mostafa A A Mahmoud)  [10.21608/AELS.2022.127212.1007](https://doi.org/10.21608/AELS.2022.127212.1007)

Received: 13 March 2022, Revised: 8 April 2022

Accepted: 9 April 2022; Published: 1 July 2022

reaction [10, 11]. Farahmand et al. [9] established the impact of coating with Mo and SDS inhibitor on mild steel in 3.5% NaCl solution. The good efficacy was noticed at SDS of 0.8 mM and Mo of 75 mm thickness. Nam et al. [13] studied the corrosion mitigation of cerium hydroxycinnamate compounds on mild steel in 0.6 M NaCl solution. Less corrosion attack occurs on the surface of the mild steel exposed to the inhibitor in contrast to the surface where the inhibitor is absent. This is as a result of a protective film caused by the action of the cerium hydroxycinnamate compounds. The result referred that cerium hydroxycinnamate compounds decreases the rate of corrosion in 0.6 M NaCl solution, and also minimize protective and magnitude of the CPE double layer, promote the charge and protective resistances. Other studies have also reported the use of various method of protection of mild steel in NaCl solutions [14–20].

The postulated inhibitory mechanism might be a combination of the van der Waals electrostatic interaction between the charged inhibitor molecules and charged metal, vacant d-orbitals of iron and the inhibitor molecules through  $\pi$ -electrons, or a combination of these processes [21]. The majority of organic inhibitors used are poisonous, costly, and unfriendly to the environment [22–26]. On the other hand, resorcinol is a safe compound used as an antiseptic and disinfectant in topical pharmaceutical drugs. Furthermore, resorcinol is inexpensive, widely available, non-toxic, and environmentally benign. Because of these characteristics, resorcinol derivatives were selected for corrosion studies.

The novelty in the present work is to examine the inhibitive properties of resorcinol derivative, DIH, towards steel in HCl media, as the synthesized compound has a high molecular mass and contains many electron donating atoms. The major objective of the conducted paper is to investigate the efficiency of the DIH compound in a 0.5 mol L<sup>-1</sup> HCl solution to decrease corrosion of CS. Weight loss (WL), electrochemical impedance spectroscopy (EIS), and potentiodynamic polarization (PP) techniques are used to examine if the DIH compound can be used as a safe and cheap inhibitor for carbon steel corrosion in 0.5 mol L<sup>-1</sup>

HCl. The rate of corrosion has been computed and discussed in relation to temperatures and thermodynamic parameters. Furthermore, the interaction between the DIH molecules and the CS was described using Monte Carlo simulation and density functional theory (DFT). The dual effect of the DIH compound on pitting and microbial corrosion due to SRB bacteria was estimated to inhibit the growth of bacteria in Postgate B media [27] (Killing test). The molecular docking simulation confirmed the in-vitro data when compared with the co-crystallized ligand in the Moe and Chimera programmes by loading PDBID= 4dnx [28].

## 2. Experimental details

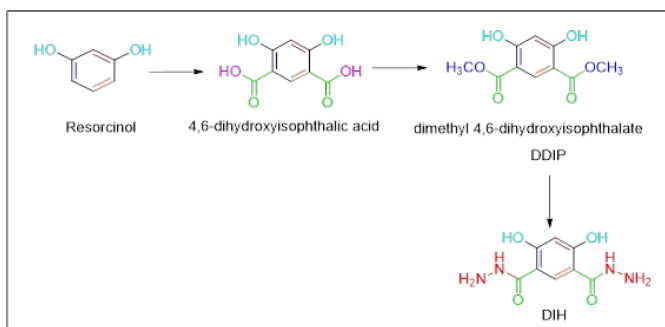
### 2.1. Materials and solutions

A CS plate with a composition (wt. %) of 0.20% C, 0.60% Mn, 0.04% P, 0.003% Si, and the rest Fe was subjected to corrosion testing. The inhibitor was used at concentrations of 50, 100, 150, 200, 250, and 300 ppm. Corrosive media were made by diluting AR grade 37 % HCl in distilled water to 0.5 mol L<sup>-1</sup> HCl. The main chemicals utilized in the preparation are resorcinol, sodium carbonate, acetone, ethanol, and methanol, all purchased from Sigma-Aldrich. As reference and counter electrodes, saturated calomel (SCE) and Pt gauze have been utilized, respectively.

### 2.2. Synthesis of resorcinol derivative, DIH

The DIH compound was prepared by dissolving 10 g of 4, 6-Dihydroxy-isophthalic acid in 100 ml of absolute MeOH, and 5 ml of conc. H<sub>2</sub>SO<sub>4</sub> was added dropwise to the solution. The mixture was refluxed in the water bath for 6 hours, and then cooled to room temperature, and the mix was poured in Na<sub>2</sub>CO<sub>3</sub> solution, filtered, and the ppt was crystallized from ethanol with a yield of 78 %. DIH compound was synthesized by reacting dimethyl 4, 6-dihydroxyisophthalate (DIH) with 10 ml of hydrazine hydrate in 50 ml of methanol. The mixture was refluxed for 6 hours, filtered, and crystallized from the methanol. The yield is 86 %. Scheme 1 shows the derivative's schematic preparation. The <sup>1</sup>H NMR spectra are shown in Figure 1.





Scheme 1: Synthesis of organic compound DIH based on resorcinol

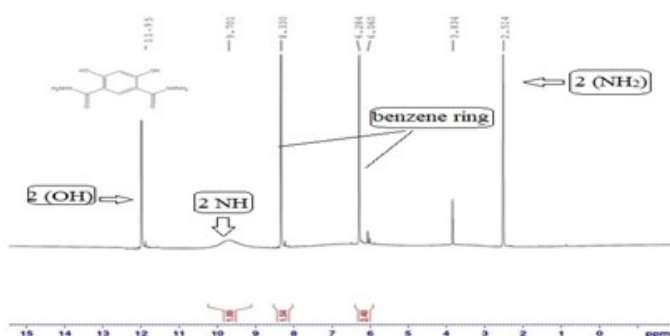


Figure 1:  $^1\text{H-NMR}$  of the DIH compound

### 2.3. Weight Loss Measurements

The gravimetric measurements were carried out using recognized methodologies [29]. In the first phase, the specimens were polished with various emery sheet grades (400–2000), rinsed with distilled water, sonication, washed in acetone, left to dry at room temperature, and then weighted. Next, the steel specimens were immersed in  $0.5 \text{ mol L}^{-1}$  HCl with and without various dosages of inhibitor for 24 hours at room temperature. This was followed by a complete cleaning technique that included ultrasonic washing in acetone, drying, and weighing the steel samples. The volume of solution is 100 ml, and the immersion times for the WL are 60, 120, 180, 240, 300, and 360 minutes at 25, 35, 45, and  $55^\circ\text{C}$ , respectively. To ensure optimal reproducibility, three CS sheets were tested simultaneously, and the mean WL value was recorded.

### 2.4. Electrochemical studies

A three-electrode cell was applied to determine the electrochemical data in this study.  $1 \text{ cm}^2$  carbon steel electrode is used as a working electrode. The saturated calomel electrode (SCE) and a platinum electrode are used as a reference and auxiliary electrodes. Electrochemical measurements were carried out with the help of a Biologic SP-150 potentiostat and the EC-LAB software. Before conducting the electrochemical tests, the working electrode was immersed in 0.5% HCl for 30 minutes. The open-circuit potential (OCP) could be established without and with varied dosages of the inhibitor. At a scan rate of  $0.2 \text{ mV s}^{-1}$ , the potentiodynamic polarization curves swept from  $-900$  to  $-100 \text{ mV}$  (vs. SCE). Analyzing electrochemical impedance is possible through the use of EIS. Using an alternating current signal at OCP with an amplitude of 5 mV and frequency ranges between 100 kHz and 0.05 Hz, the EIS measurements were made. The findings were averaged over three trials for each test. A personal computer was used to acquire the data. The data was displayed, graphed, and fitted using Origin 2018 and Microsoft Office 2016 programmes.

### 2.5. Surface analysis study

The CS surface was handled with various abrasive sheets (grades 250 to 1200). The coupons were then rinsed with deionized water before being immersed in  $0.5 \text{ mol L}^{-1}$  HCl for 48 hours in the non-existence and existence of the examined organic compound's optimal concentration (300 ppm). The coupons were then treated with deionized water, dried, and inserted into the spectrometer with no additional processing. A JOEL JSM-6510 LV scanning electron microscope (SEM) and atomic force microscopy (AFM) (Model: Keysight 5600LS large stage, made in the USA) were used to get the images [30].

### 2.6. Calculations involving quantum chemistry

The quantum chemical parameters were determined using the DFT/6-31+G (d, p) basis set and Monte Carlo MP<sub>2</sub> functional with a 3-21G (d) basis set for all atom simulations.

## 2.7. Biological Activity Evaluation

### 2.7.1. In Vitro

The antibiotic effect of the synthesized organic compound DIH on the sulfate-reducing bacteria (SRB) in oil and gas fields was assessed using the serial dilution method according to the American Society for Testing and Materials (ASTM) designation (D 4412-84) [31]. Water contaminated by SRB was supplied by the General Petroleum Company (G.P.C, Western Desert, Egypt). The SRB was treated with a dosage of the organic chemical produced (50, 150, and 300 ppm). The system was kept in the incubator for 3 hours. Each system was grown for 21 days at a temperature of 37 - 40 ° C using an SRB-specific medium.

### 2.7.2. In Silico (Virtual mechanism by Molecular Docking)

The virtuality of the structural bioinformatics research towards the active sites of the structure of the ATP sulfurylase ligand, which was retrieved from the Protein Data Bank, under the designation (PDB = 4DNX), was used to elucidate the virtual method of binding of the produced compounds. Chemically and energetically, all of the substances studied were improved. Furthermore, Nafie et al. 2019 [20] stated that the protein structure was publicly available from the PDB and optimized using standard procedures. MOE 2019 was used to verify molecular docking calculations, while Chimera was used as a visualization programmer to investigate drug-target interactions.

## 3. Results and discussion

### 3.1. WL study

To study the effect of introducing DIH at various concentrations on the corrosion of carbon steel, the WL technique was used after six hours of immersion at 25 °C in 0.5 mol L<sup>-1</sup> of HCl. The WL is determined as the weight of the CS, which dissociates when the carbon steel specimen is corroded in the corrosive medium and is calculated from equation (1):

$$\Delta W = W_1 - W_2 \quad (1)$$

DW is the WL of the carbon steel specimen, and W<sub>1</sub> and W<sub>2</sub> are the CS weights before and after

being treated with 0.5 mol L<sup>-1</sup> HCl, respectively. The corrosion rate (CR) and inhibition efficiency IE<sub>WL</sub> (%) were calculated according to the following equation (2):

$$CR = \Delta W / At \quad (2)$$

Where ΔW denotes the WL value, A denotes the total area per cm<sup>2</sup>, and t signifies the time of immersion in minutes. Table 1 shows the results of CS tests in 0.5 mol L<sup>-1</sup> HCl acid with and without various concentrations of the DIH compound. The compound's inhibitory effectiveness improves with increasing its concentration in the corrosive solution.

### 3.2. The impact of temperature on inhibition efficacy

The impact of solution temperature on the inhibitory efficacy is evaluated at 25, 35, 45 & 55 °C, and the data are reported in Tables 2 and 3. The efficacy of inhibition lowers as temperature rises. With increasing temperature, the inhibitor molecules depart the steel surface, resulting in a decrease in inhibition efficacy values.

### 3.3. The thermodynamic activation parameters of the corrosion process

Thermodynamic parameters are crucial and significant tools for understanding inhibitor adsorption behaviour. The activation energy (E<sub>a</sub><sup>\*</sup>), enthalpy change (ΔH<sub>a</sub><sup>\*</sup>), and entropy change (ΔS<sub>a</sub><sup>\*</sup>) of activation for the dissolution of CS in 0.5 mol L<sup>-1</sup> HCl solution were estimated. Arrhenius and transition-state equations were used to calculate the parameters in the non-existence and existence of various doses of the DIH chemical compound.

$$K = A \exp\left(\frac{E_a^*}{RT}\right) \quad (3)$$

$$\ln\left(\frac{k}{T}\right) = \left(\ln\left(\frac{k_B}{h}\right) + \left(\frac{\Delta S_a^*}{R}\right)\right) - \frac{\Delta H_a^*}{RT} \quad (4)$$

Where k is the dissolution rate, R is the gas constant, k<sub>B</sub> is the Boltzmann constant, T is the Kelvin temperature, and h indicates Planck's constant. The Arrhenius plot (log k vs. 1/T) and transition-state plots (log k/T vs. 1/T) of the DIH compound

Table 1: Data of WL measurements for carbon steel in 0.5mol L<sup>-1</sup> HCl solution without and with different concentrations of the DIH compound at 25 °C. The immersion time is 240 min.

Concentration (ppm)	DIH		
	CR Kg.m <sup>-2</sup> .s <sup>-1</sup> x 10 <sup>-9</sup>	$\theta$	IE%
Blank	78.5±0.2	...	...
50	28.8±0.3	0.633	63.3±0.2
100	26.2±0.1	0.666	66.6±0.1
150	23.3±0.4	0.703	70.3±0.4
200	20.0±0.5	0.745	74.5±0.2
250	17.9±0.1	0.772	77.2±0.1
300	15.0±0.2	0.809	80.9±0.3

Table 2: Carbon steel corrosion rate after immersion in 0.5mol L<sup>-1</sup> HCl without and with different concentrations of the DIH compound at different temperatures.

Concentration (ppm)	DIH			
	CR, Kg.m <sup>-2</sup> .s <sup>-1</sup> x10 <sup>-9</sup> at 240 min.			
	25 °C	35 °C	45 °C	55 °C
Blank	78.00±0.2	80.00±0.1	83.00±0.2	86.00±0.5
50	28.81±0.2	32.50±0.1	36.25±0.3	42.08±0.5
100	26.23±0.3	29.58±0.3	34.17±0.4	38.75±0.4
150	23.32±0.4	26.25±0.2	30.83±0.1	35.42±0.1
200	20.12±0.1	24.17±0.2	28.33±0.5	32.92±0.2
250	17.96±0.5	20.42±0.4	25.83±0.2	30.42±0.2
300	15.20±0.1	19.17±0.4	20.42±0.3	25.00±0.3

Table 3: Data of WL measurements at 240 min for carbon steel in 0.5mol L<sup>-1</sup> HCl without and with different concentrations of DIH compound, at different temperatures.

DIH											
25 °C			35 °C			45 °C			55 °C		
Concn. (ppm)	$\theta$	%IE	Concn. (ppm)	$\theta$	%IE	Concn. (ppm)	$\theta$	%IE	Concn. (ppm)	$\theta$	%IE
0	...	...	0	...	...	0	...	...	0	...	....
50	0.633	63.3±0.2	50	0.589	58.95±0.1	50	0.554	55.38±0.1	50	0.512	51.21±0.2
100	0.666	66.6±0.1	100	0.626	62.63±0.3	100	0.579	57.95±0.1	100	0.551	55.07±0.3
150	0.703	70.3±0.4	150	0.668	66.84±0.5	150	0.621	62.05±0.3	150	0.589	58.94±0.2
200	0.745	74.5±0.3	200	0.695	69.47±0.4	200	0.651	65.13±0.4	200	0.618	61.84±0.4
250	0.772	77.2±0.2	250	0.742	74.21±0.2	250	0.682	68.21±0.5	250	0.647	64.73±0.5
300	0.809	80.9±0.3	300	0.758	75.79±0.1	300	0.749	74.87±0.3	300	0.710	71.01±0.1

Table 4: Activation parameters for dissolution of CS without and with different concentration of the compound DIH in 0.5 mol L<sup>-1</sup> HCl.

Concentration (ppm)	E <sub>a</sub> <sup>*</sup> (kJ mol <sup>-1</sup> )	R <sup>2</sup>	ΔH <sup>*</sup> (kJ mol <sup>-1</sup> )	ΔS <sup>*</sup> (J mol <sup>-1</sup> K <sup>-1</sup> )
Blank	3.5	0.94	0.9	-263
50	10.2	0.98	7.6	-252
100	10.6	0.98	8.0	-251
150	10.6	0.99	8.0	-53
200	11.1	0.99	8.5	-52
250	12.2	0.95	9.6	-49
300	12.9	0.95	10.2	-47

Table 5: Equilibrium constant K<sub>ads</sub> and standard free energy ΔG<sup>o</sup><sub>ads</sub> of adsorption of the compound DIH on CS in 0.5 mol L<sup>-1</sup> HCl at different temperatures.

Temperature (°C)	DIH				
	Slope	Intercept x 10 <sup>-5</sup>	K <sub>ads</sub> x 10 <sup>-3</sup> (mol <sup>-1</sup> )	ΔG <sup>o</sup> (KJ/mol)	R <sup>2</sup>
25	1.22	81.7	1223.5	-27.6	0.99
35	1.29	92.8	1076.9	-26.8	0.99
45	1.32	94.1	1064.2	-26.8	0.99
55	1.41	46.7	2143.1	-28.5	0.99

Table 6: Potentiodynamic polarization parameters of carbon steel in 0.5 mol L<sup>-1</sup> HCl containing different concentrations of the compound DIH at 25°C

Compd. DIH (ppm)	-E corr (V vs SCE) x 10 <sup>-3</sup>	β <sub>a</sub> (V dec <sup>-1</sup> ) x 10 <sup>-3</sup>	-β <sub>c</sub> (V dec <sup>-1</sup> ) * 10 <sup>-3</sup>	I corr (A /cm <sup>2</sup> ) * 10 <sup>-3</sup>	θ	%IE
Blank	391	242	322	1.52	....	...
50	401	207	298	0.58	0.618	61.8±0.2
100	387	201	221	0.52	0.658	65.8±0.1
150	394	197	200	0.42	0.724	72.4±0.3
200	391	185	189	0.35	0.770	77.0±0.4
250	392	165	183	0.28	0.816	81.6±0.5
300	382	121	141	0.20	0.868	86.8±0.2

are shown in Figure 2. The Arrhenius plot creates a straight line with a slope of  $-E_a^*/2.303R$ , through which the  $E_a$  value of the impeded dissolution process of CS is evaluated and listed in Table 4. The  $E_a^*$  has a value of 3.5 kJ mol<sup>-1</sup> for the blank solution. Because the DIH compound inhibits the corrosion process, the activation energy significantly increases with varying concentrations of the or-

ganic compound. This change in  $E_a$  might be attributed to either DIH compound precipitation on the CS surface or a change in the potential difference of the metal solution border due to adsorption. Transition-state plots show straight lines with slopes of  $(\Delta H_a^*/2.303R)$  and intercept  $\log(k_B/h) + \Delta S_a^*/R$ , from which the  $\Delta S_a^*$  and  $\Delta H_a^*$  quantities in Table 4 were. The positive  $\Delta H_a^*$  indicates that

Table 7: EIS data of carbon steel in 0.5 mol L<sup>-1</sup>HCl without and with different concentration of the compound DIH at 25°C.

Concn. (ppm)	Rct (Ω cm <sup>2</sup> )	Rs (Ω cm <sup>2</sup> )	Yo m Ω <sup>-1</sup> sn cm <sup>-2</sup>	DIH		C <sub>d</sub> l x10 <sup>-6</sup> (F cm <sup>-2</sup> )	θ	IE%
				n	χ <sup>2</sup> ×10 <sup>3</sup> %			
Blank	48.60	1.44	0.150	0.98	5.57	108	...	...
50	129.1	1.46	0.135	0.87	7.41	40	0.624	62.4±0.3
100	140.4	1.45	0.098	0.87	8.18	35	0.654	65.4±0.1
150	180.1	1.53	0.071	0.78	6.03	24	0.730	73.0±.04
200	220.8	1.52	0.061	0.85	8.68	20	0.779	77.9±0.2
250	280.3	1.62	0.053	0.88	6.45	15	0.827	82.7±0.1
300	351.3	1.48	0.180	0.89	5.45	13	0.862	86.2±0.4

Table 8: AFM parameters of carbon steel.

Substance	Sa (μm)	Sq(μm)	Sp(μm)	Sv(μm)	Sz(μm)
Control	0.0451	0.0616	0.234	0.436	0.670
0.5 mol L-1 HCl	0.254	0.351	6.04	3.56	9.60
DIH	0.138	0.203	0.759	1.41	2.17

Table 9: The calculated quantum chemical parameters obtained from DFT theory

HOMO	UMO	ΔE	D	η	σ	μ	χ	ω	Total negative charge TNC	Total energy (Et)	Volume (cm <sup>3</sup> /mol)
(a.u)	(a.u)	(a.u)	(Debye)	(a.u)	(a.u)	(a.u)	(a.u)	(a.u)			
-	-	0.195	7.974	0.098	10.20	-0.15	0.15	0.12	-6.89	-830.76	153.47
0.25	0.05										

Table 10: The descriptors calculated by the Monte Carlo simulation for adsorption of the inhibitors on Fe(110) surface

Molecule	Total Energy (kcal/mol)	Adsorption Energy (kcal/mol)	Deformation Energy (kcal/mol)	Rigid adsorption Energy (kcal/mol)
DIH	-29.010	-128.310	-23.295	-105.014

Table 11: Biocide effect of the investigated synthetic compound against SRB

Conc. Compd.	50 ppm (cell/ml)	150 ppm (cell/ml)	300 ppm (cell/ml)
Blank		106	
DIH	104	102	Nil

an endothermic mechanism forms the activation

complex. The negative of  $\Delta S_a^*$  indicates that the DIH molecules were ordered on the CS surface, resulting in a reduction in entropy [32].

### 3.4. Adsorption considerations

Both chemical and physical adsorption mechanisms are involved in the (CS)/inhibitor relationship adsorption process. The metal's charge, the examined molecule's chemical structure, and the electrolyte's aggressiveness, all play a role here.



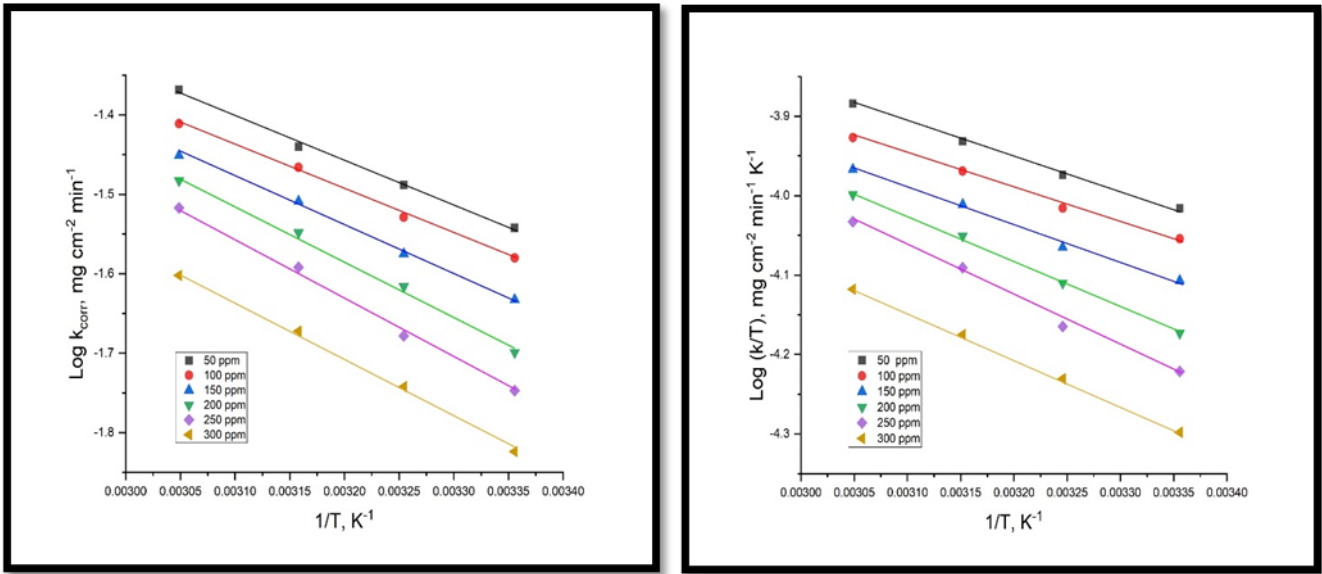


Figure 2: Arrhenius plots (log k vs. 1/T) and Transition-state plots (log k/T vs. 1/T) for corrosion of carbonsteel in 0.5 mol L<sup>-1</sup> HCl without and with different concentrations of the compound DIH.

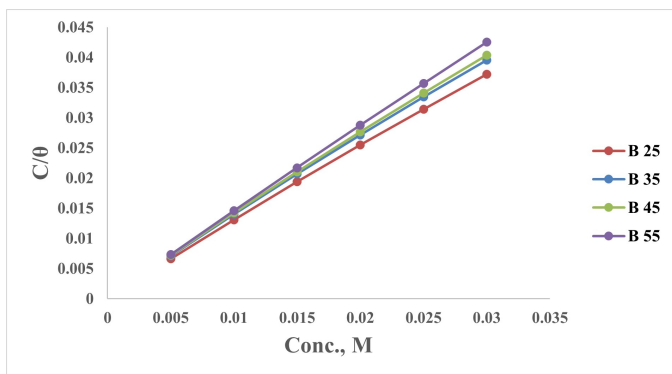


Figure 3: Langmuir adsorption isotherms for the compound DIH on carbon steel in 0.5 mol L<sup>-1</sup> HCl at different temperatures.

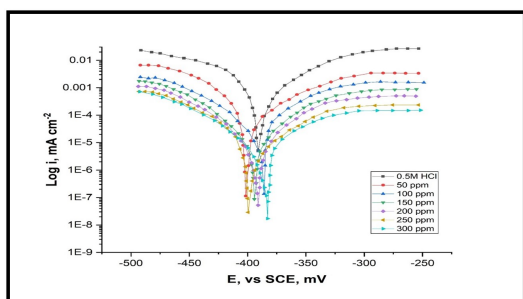


Figure 4: Plots of potentiodynamic polarization for dissolution of carbon steel without and with different concentrations of compound DIH, at 25°C.

Compared to alternative adsorption models, the Langmuir model is the best-suited isotherm for describing the adsorption behavior of the investigated inhibitor, with a regression coefficient of  $R^2 = 0.9994$ . (Frumkin, Freundlich, and Temkin). Langmuir may be determined using the following formula

$$\frac{C}{\theta} = \frac{1}{K_{ads}} + C \quad (5)$$

Where C is the inhibitor concentration, and  $K_{ads}$  is the constant of equilibrium adsorption-desorption process on the CS surface, respectively, and ( $\theta$ ) is the electrochemically determined (CS) surface coverage. Figure 3 depicts a linear relationship with a slope and a correlation coefficient close to one. Additionally, the fitted data from both measures (potentiodynamic polarization and weight loss) are connected. The ( $K_{ads}$ ) value appears using the free energy standard of adsorption ( $G^{\circ}_{ads}$ ). [33–35] (6):

$$K_{ads} = \frac{1}{55.5} \exp\left(\frac{-\Delta G^{\circ}}{RT}\right) \quad (6)$$

Where 55.5 denotes the molar amount of H<sub>2</sub>O. The negative value of  $\Delta G^{\circ}_{ads}$  confirmed that the CS surface has a long-lasting adsorption coating [36]. The physisorption process is defined as  $\Delta G_{ads}$  values up to 20 kJ mol<sup>-1</sup>. Those greater than 40 kJ mol<sup>-1</sup> are, however, chemisorption [37], [38]. For the present system, the  $\Delta G^{\circ}_{ads}$  is ranged between

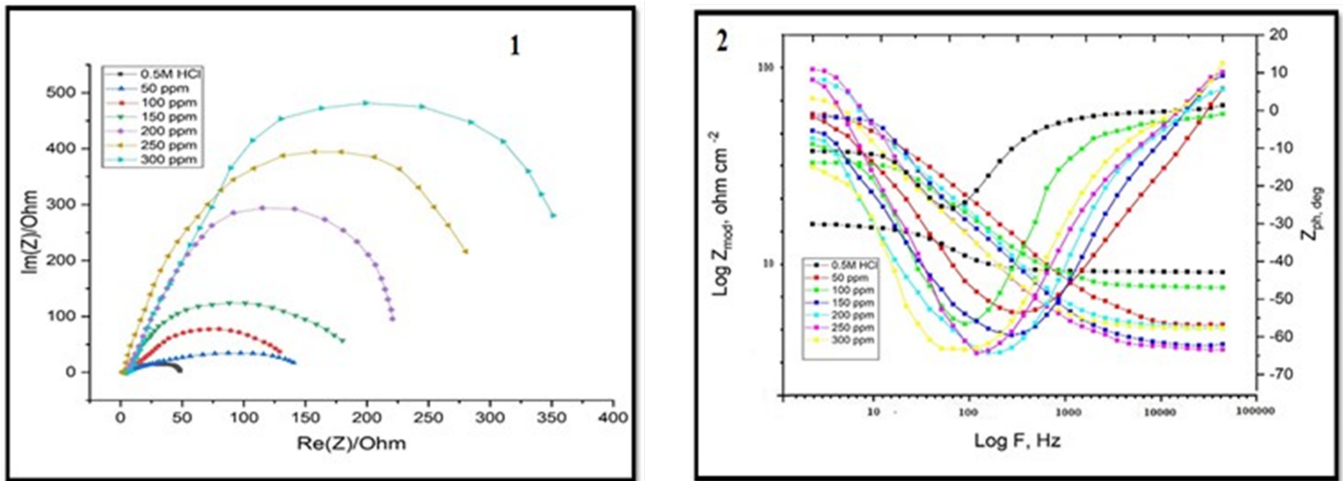


Figure 5: The Nyquist (1) and Bode(2) plots for the corrosion of carbon steel in 0.5 mol L<sup>-1</sup> HCl without and with different concentrations of DIH at 25°C

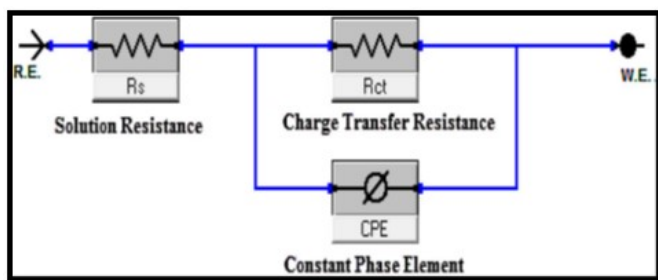


Figure 6: Equivalent circuit model used to fit experimental EIS data

-27.6 and - 28.5 kJ mol<sup>-1</sup>. The DIH inhibitor, as shown in Table 5 , reduces the rate of CS corrosion via physisorption and chemisorption processes.

3.5. PP measurements

The Tafel polarization curves for CS in 0.5 mol L<sup>-1</sup> HCl acid at varied DIH concentrations are shown in Figure 4. Table 6 lists all of the electrochemical properties, including corrosion potential ( $E_{corr}$ ), corrosion current density ( $i_{corr}$ ), Tafel anodic slope ( $\beta_a$ ), and Tafel cathodic slope ( $\beta_c$ ). The inhibitory effectiveness was calculated using Eq. (7).

$$\%IE = \theta \times 100 = \frac{(i^o_{corr} - i_{corr})}{i^o_{corr}} \quad (7)$$

The current densities that are unregulated and inhibited are given by  $i^o_{corr}$  and  $i_{corr}$ , respectively.

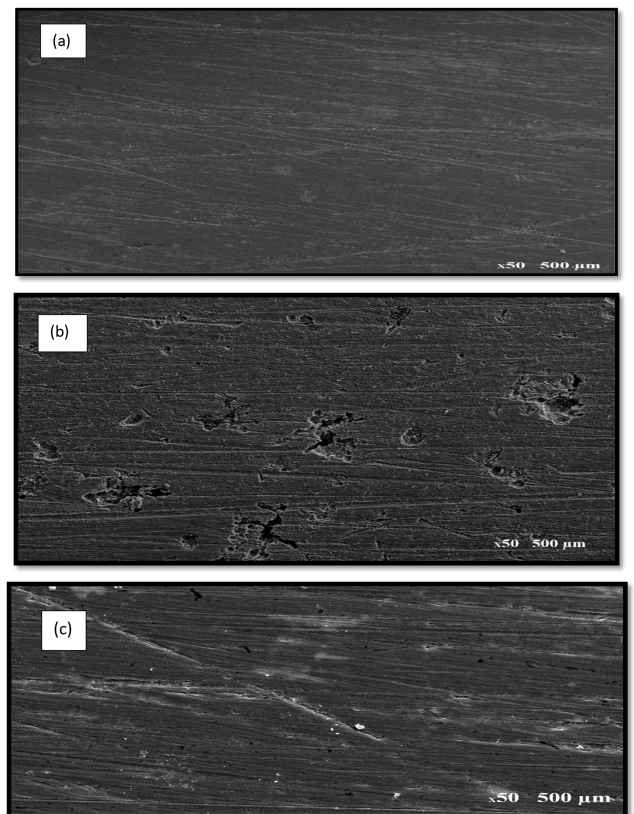


Figure 7: a) Pure CS surface; b) CS after immersing in 0.5mol L<sup>-1</sup> HCl; and d) CS after immersing in 0.5 mol L<sup>-1</sup> HCl+ 300 ppm DIH

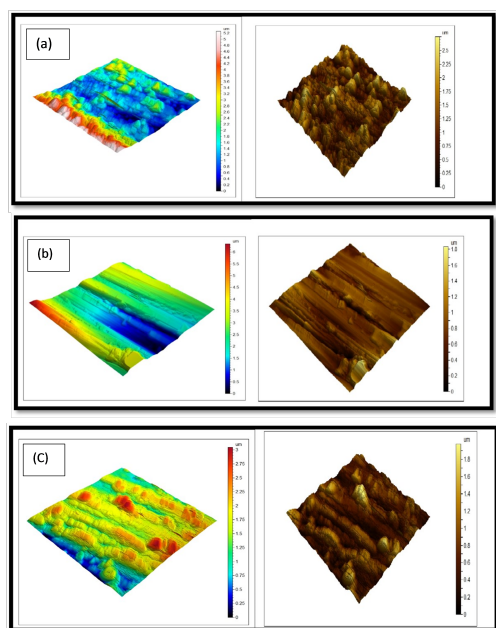


Figure 8: a) AFM three-dimensional picture of pure carbon steel; b) AFM three-dimensional picture of carbon steel surface after immersion for 48 hours in 0.5 mol L<sup>-1</sup> HCl; c) AFM three-dimensional picture of carbon steel after immersion for 48 hours in 0.5 mol L<sup>-1</sup> HCl + 300 ppm DIH.

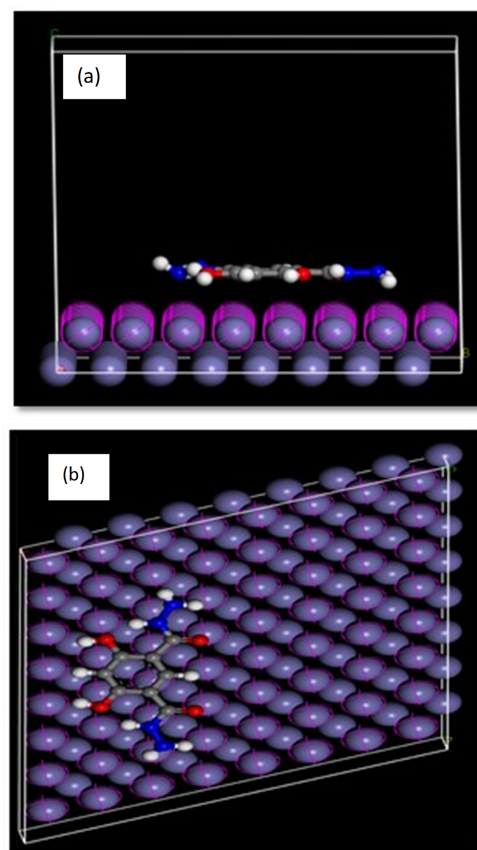


Figure 10: (A) Side view and (B) Top view for adsorption of investigated inhibitor on Fe (110).

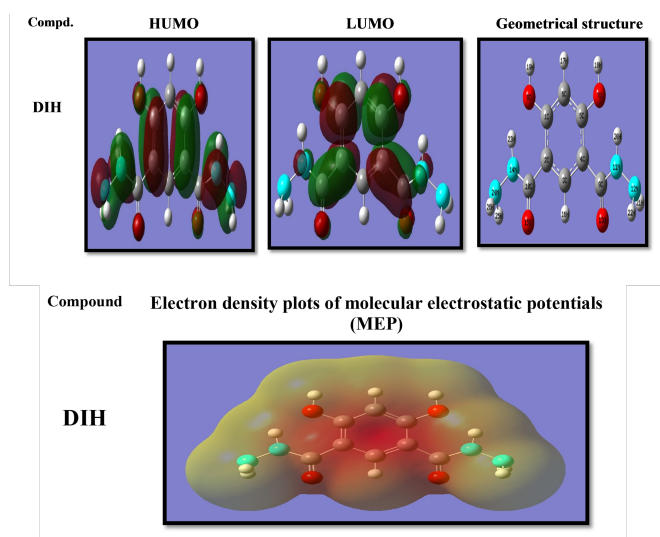


Figure 9: Geometrical structure and charge density distribution of HOMO and LUMO levels of the inhibitor compound DIH.

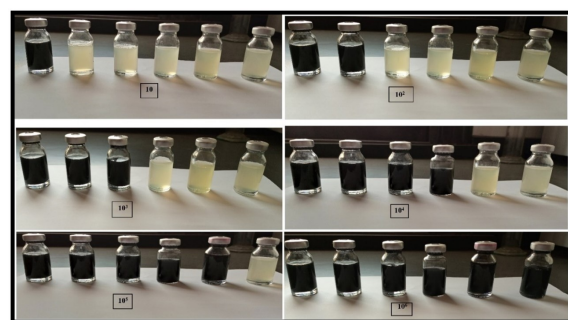


Figure 11: Counted SRB media after 21 incubation day.

The corrosion potential ( $E_{corr}$ ) and corrosion current density ( $i$ ) got from the intersection of the cathodic, and anodic polarization curves are listed in Table 6 . The corrosion current density ( $i$ ) was measured using the subsequent equation:

$$i = B / R_p \quad (8)$$

Where  $R_p$  is that the polarization resistance &  $B$  is that the Stern–Geary constant, calculated by the following equation:



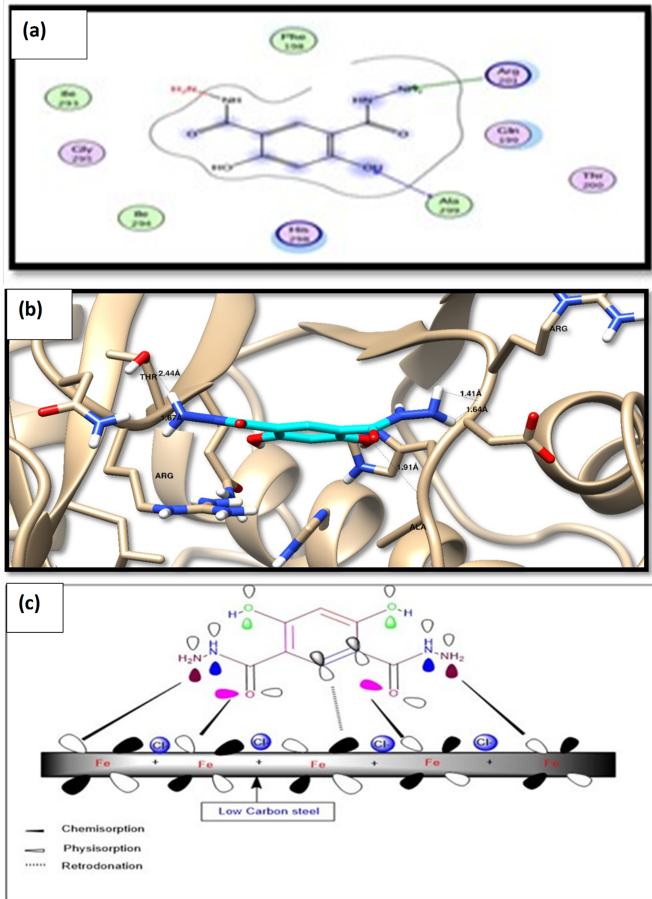


Figure 12: a) Ligand-receptor interactions of the docked DIH compound inside the active site of the structure of the ATP sulfurylase (PDB=4DNX); b) The three dimensional (3D) binding position of compound DIH inside the active site of the structure of the ATP sulfurylase (PDB=4DNX); c) Suggested adsorption of DIH compound on the LCS surface.

$$B = \frac{\beta_a \beta_c}{2.303(\beta_a + \beta_c)} \quad (9)$$

Where:  $\beta_a$  and  $\beta_c$  are the anodic and cathodic Tafel slopes, respectively.

As shown in Figure 4 and Table 6, the corrosion potential ( $E_{corr}$ ) values have altered somewhat. The difference in corrosion potential ( $E_{corr}$ ) between the absence and presence of the investigated inhibitor is fairly small, indicating that the inhibitor is a mixed-type inhibitor that accords with open circuit potential measurements [39]. In addition, the anodic and cathodic Tafel slopes change, showing that the inhibitor is a mixed inhibitor that controls both anodic and cathodic processes. These effects might be caused by inhibitor

molecules adsorbing on the CS surface [40], [41]. As seen in Table 5, the  $i_{corr}$  decreases as the inhibitor concentration increases. As the inhibitor concentration is raised, the inhibition efficiency increases till attaining 86.8% at 300 ppm.

### 3.6. EIS measurements

Table 7 summarizes the data derived from EIS measurements for the dissolution of CS in the presence of the DIH compound and 0.5 mol L<sup>-1</sup> HCl acid at room temperature. The Nyquist (1) and Bode (2) plots for CS in 0.5 mol L<sup>-1</sup> HCl in the non-existence and existence of varying dosages of the DIH compound are depicted in Figure 5. The impedance spectra demonstrate only one semicircle. The semicircle suggests that the dissolution of CS in 0.5 mol L<sup>-1</sup> HCl acid is mainly governed by a charge transfer and is often associated with the charge transfer and double-layer nature of the corrosion process [42]. In the presence of DIH, the diameter of the capacitive loop is larger than in the case of an inhibitor-free solution and increases with DIH dosage. This implies that as the inhibitor dose increases, so does the impedance of the inhibited substrate. The frequency dispersion effect may be seen because these impedance spectra are not perfectly symmetrical semicircles. This abnormal behavior is commonly attributed to the imperfections and non-uniformity of the CS surface [43]. As seen in Figure 5 (2), the impedance spectra in the Bode plots show only one semicircle correlating to one time constant. It is reasonable to conclude that when the inhibitor dose increases, the charge transfer resistance  $R_{ct}$  value increases, while double-layer capacitance ( $C_{dl}$ ) values drop. The most likely causes of this effect are a reduction in the local dielectric constant and/or a growth in the thickness of the double layer [44]. The equivalent circuit shown in Figure 6 is being used to analyze the Nyquist curves, which comprise  $R_s$  and CPE (constant phase element) parallel to the  $R_{ct}$ .

The variables such as a proportional factor ( $Y_0$ ), phase shift ( $n$ ),  $R_s$ , &  $R_{ct}$  were calculated with the help of the ZSimpWin program. The impedance variables are given in Table 7. The CPE type impedance,  $Z_{CPE}$ , was estimated from the

subsequent equation:

$$Z_{CPE} = \frac{1}{Y_o(j\omega)^n} \quad (10)$$

Where  $n$  is that the phase shift, that enables notification for the degree of imperfection in capacitive action, and  $Y_o$  is a proportionality operator,  $j = \sqrt{-1}$  and  $\omega = 2\pi f$ .

Double-layer capacitance magnitudes ( $C_{dl}$ ) obtained from CPE parameters in keeping with the subsequent relation:

$$C_{dl} = Y_o(\omega_{max})^{n-1} \quad (11)$$

Where  $\omega_{max} = 2\pi f_{max}$  and  $f_{max}$  is that the frequency when the imaginary part of the impedance is the utmost.

The mitigation efficacy of surfactant can be estimated via the next equation:

$$IE\% = \frac{R_{ct}^o - R_{ct}}{R_{ct}^o} \times 100 \quad (12)$$

Where,  $R_{ct}$  and  $R_{ct}^o$  are the electron-transfer resistances magnitudes in the non-existence & existence of the prepped compound, respectively.

For Bode plots, there is a directly proportional relation between  $\log |Z|$  and  $\log f$ . The value of a slope approaches -1 & the phase angle value adjacent to  $-65^\circ$ . This proves the non-ideal capacitive performance at mediate frequencies. It was reported that the perfect capacitive performance is attained if the slope is -1 & the angle of phase is  $-90^\circ$  at mediate frequencies. The magnitudes of slope and phase angle in inhibited solutions are larger than ones get in uninhibited solution. This confirms the mitigation performance of the examined compound in the disintegration process of steel. Increasing the amount of the prepped compound in the corroding solution improves the inhibition efficacy because of the adhesion of more surfactant molecules at the metal surface.

It is worth observing that the magnitudes of mitigating efficiency estimated by PP and EIS methodologies differ just a little. Indeed, the discrepancies between the two methods are attributed to variations in the surface state of the electrode material [45].

### 3.7. Surface Studies

SEM and AFM techniques reveal a CS surface's smoothness and decreased roughness in the presence of the synthetic chemical DIH.

#### 3.7.1. SEM investigation

Figure 7 a shows an SEM image of the polished surface of CS before immersion in the test solution of  $0.5 \text{ mol L}^{-1}$  HCl. Figures 7b and 7c show the micrographs of CS specimens without and with 300 ppm of the DIH organic compound after 48 hours of exposure to  $0.5 \text{ mol L}^{-1}$  HCl solution at room temperature. The CS surface of the blank specimen is severely corroded. however, in the presence of the DIH compound, the surface is smoother and has less roughness influenced by the corrosion process than the blank solution. The surface became isolated from the corrosive medium because of the adsorption of the synthetic compound on the CS surface and the formation of a protective film. As a result, the organic compound is an effective CS corrosion inhibitor in HCl media.

#### 3.7.2. AFM characterization

AFM is utilized to test the surface appearance at the pico to micro-scales, which is a stunning and innovative tool for examining the effect of the inhibitors on the corrosion process at the CS/solution boundary. Figure 8 show three-dimensional (3D) AFM morphologies for CS in  $0.5 \text{ mol L}^{-1}$  HCl in the presence and absence of the optimum concentration (300 ppm) of the DIH compound after 48 hours of room temperature. The surface of the CS in  $0.5 \text{ mol L}^{-1}$  HCl is significantly more damaged than the surface of the CS in the presence of the organic compound. The CS surface in  $0.5 \text{ mol L}^{-1}$  HCl acid is significantly more damaged than the CS in the presence of the organic compound. In addition, the average roughness of CS in  $0.5 \text{ mol L}^{-1}$  HCl solution (blank) is calculated to be  $0.254 \mu\text{m}$ . In the presence of the DIH compound, the mean roughness is reduced to  $0.155 \mu\text{m}$ , implying that the studied organic compound is adsorbed at the CS surface and constitutes a protective film that isolates the CS surface from the aggressive HCl solution. All height parameters are given in Table 8 , such as the arithmetic



mean height (Sa), the root mean square height (Sq), the maximum peak height (Sp), the maximum pit height (Sv), and the maximum height (Sz), are computed in micrometer units according to ISO 25178 [46]. The inhibitory efficacy output data from chemical and electrochemical approaches agrees well with the roughness values obtained.

### 3.8. DFT results

The nature of the interaction between the DIH compound's adsorption centers and the CS surface was investigated using DFT simulations. Figure 9 a shows the optimized structure's highest occupied (HOMO) and lowest unoccupied (LUMO) molecular orbitals. The energy gap ( $\Delta E$ ) between  $E_{HOMO}$  and  $E_{LUMO}$  is calculated. Other factors affecting the nature of the DIH-CS relationship, like ionization potential (I), electron affinity (A), electronegativity ( $\chi$ ), chemical potential ( $\mu$ ), hardness ( $\eta$ ), softness ( $\sigma$ ), electrophilicity ( $\omega$ ), total negative charge, total negative charge (TNC) and total energy ( $E_t$ ) were estimated by the subsequent relationships [46] and are listed in Table 9.

$$\Delta E = E_{LUMO} - E_{HOMO} \quad (13)$$

$$I = - E_{HOMO} \quad (14)$$

$$A = - E_{LUMO} \quad (15)$$

$$\mu = - \chi \quad (16)$$

$$\mu = \frac{(E_{HOMO} + E_{LUMO})}{2} \quad (17)$$

$$\eta = \frac{(E_{LUMO} - E_{HOMO})}{2} \quad (18)$$

$$\sigma = \frac{1}{\eta} \quad (19)$$

Quantum mechanics simulations were utilized to examine the process of adsorption at the CS surface and analyze the influence of structural factors on inhibitor effectiveness. The DIH's molecular and electronic characteristics were determined by optimizing the lengths and angles of its bonds as well as the distortion angles. Figure 9 depicts the estimated configurations with the lowest energy gained from these calculations. As a result of the electron sharing between the oxygen in the DIH and the CS, the studied inhibitor may adsorb at the CS surface [47]. The computations revealed that the geometrical structures of the examined organic compound are virtually planned, as illustrated in Figure 9. It has been reported that chemical reactivity is determined by the interaction of HOMO and LUMO levels [48].

The capacity of a molecule to transfer electrons to a suitable acceptor with unoccupied molecular orbitals is denoted by EHOMO, and the ability to acquire electrons is denoted by ELUMO. The molecule's capacity to accept electrons is proportional to the value of E LUMO [49]. The higher the EHOMO value of the inhibitor, the simpler it is for it to transfer electrons to the CS's unoccupied d-orbital, and the greater the inhibitory effectiveness. As indicated in Table 9, DFT studies demonstrated that the organic inhibitor has a high EHOMO -0.248a.u. This may explain why the DIH inhibitor has high adsorption potential on the CS surface. D [50] used the dipole moment to explain and justify the structure. D is the first derivative of an applied electrical field's energy. Table 9 shows a strong correlation between D and inhibition efficiency. Another quantum parameter derived from the computations is the molecule volume. The progressive increase in inhibitor molecular volume indicates that the metal surface area covered/protected by the inhibitor molecules is gradually enhanced by extending the length of the hydrophobic chain. This observation is consistent with the findings of the polarization and impedance experiments. The inhibitor DIH has a large molecular volume of 153.470 cm<sup>3</sup>/mol. This improves the inhibitor's inhibition efficacy by expanding the surface contact between the inhibitor's molecules and the metal

surface. This is consistent with the experimental findings.  $h$  &  $s$  are significant qualities that assess a molecule's stability and reactivity, and they agree with experimental evidence.

Furthermore, the calculations revealed that the DIH inhibitor has a low  $\chi$  and  $\omega$  and a high TNC (-6.886e), Table 9, which increases its donating capability to the CS surface and, as a result, its inhibitory efficacy. The preceding section concludes that the quantum characteristics confirm that the DIH compound has a high inhibitory efficiency, which is by the experimental findings. In addition, the HOMO level of the inhibitor is mainly localized at the lone pairs of nitrogen atoms in the  $\text{NHNH}_2$  moiety and at the  $\pi$ -bonding character of the C-C bond of the phenyl moiety. This indicates that these moieties are the favorite centers for the nucleophilic attack at the CS surface, as shown in Figure 9. This also implies that the phenyl moiety, which has a high coefficient of HOMO density, was orientated towards the CS surface and that adsorption happens most likely via its  $\pi$ -electrons.

Moreover, the calculations revealed that the charge density of the LUMO level is localized as the anti-bonding character of the C-C phenyl moiety and C=O groups for the examined compound, implying that these moieties might be reacted as an electrophile, as shown in Figure 9. The molecular electrostatic potentials (MEPs) are immensely beneficial in that negative regions could be viewed as nucleophile sites, while positive electrostatic potential regions can be considered potential electrophile sites. In addition, the electrostatic potential reveals the polarization of the electron density. The results revealed that the oxygen atom has a negative electrostatic potential, implying that these centers are energetically favorable for attachment to the metal surface, Figure 9. According to the obtained results, there is a strong link between the examined inhibitor's quantum chemical characteristics and its inhibition efficacy for CS corrosion.

### 3.9. Monte Carlo simulation

The Monte Carlo (MC) technique is particularly successful for anticipating inhibitor chemical interactions and adsorption processes on the sub-

strate surface [51]. The most stable DIH molecule configuration was found on the surface of Fe (110), with the cleavage plane ( $h, k, l$ ) (i.e., 110) being the most stable for the iron crystal [52, 53]. The adsorption locator modules were in charge of the MC study, which included a three-cycle simulated annealing run with 10,000 steps each. The force field was set to compass, and the energy calculation quality was set to ultrafine. Figure 10 displays the mechanisms of DIH compound adsorption on the Fe (110) crystal from both the side and top views. The simulation approach's output data is mostly in the form of energy indicators, like the overall energy of an adsorbate is equal to the sum of its internal and adsorption energies ( $E_{tot}$ ). The adsorption energy ( $E_{ads}$ ) is calculated by adding the stiff adsorption energy to the deformation energy generated when the inhibitor molecule (adsorbate) is loosened on the low carbon steel surface (substrate). When non-relaxed adsorbate components are adsorbed on the substrate, the stiff adsorption energy ( $E_{rigid}$ ) is released (or needed). When the adsorbed inhibitor components on the low carbon steel surface relax, deformation energy ( $E_{def}$ ) is released. Table 10 shows that the DIH molecule's adsorption energy is more stable, meaning that the DIH molecule has a stronger interaction with the low carbon steel surface and hence a higher inhibitory efficiency, which is consistent with the experimental results.

### 3.10. Laboratory examination

The antibacterial action of the produced organic compound DIH on sulfate-reducing bacteria (SRB) in oil and gas fields was evaluated using the serial dilution technique according to ASTM D4412-84 [17]. SRB-contaminated water was provided by the General Petroleum Company (GPC, Western Desert, Egypt). A total of 106 bacteria cells/ml grew in the polluted water. A dosage of the synthesized organic compounds was evaluated as a biocide for the SRB (50, 150, and 300 ppm). The system was incubated for 3 hours of contact time. Then, each system was grown for 21 days at 37-40 °C in an SRB-specific medium. Table 11 and Figure 11 show the results.

Table 12: The comparison between the tested DIH and other inhibitors reported in the literature

Inhibitor name	IE (%)	Reference
4-(p-tolyldiazenyl)-2-((E)-p-tolylimino)methyl)phenol	55.0	[54]
3-(2-((4-hydroxybenzylidene)amino)thiazole-4-yl)-2H-chromen-2-one	52.9	[55]
N-(4-N,N-dimethylaminobenzal)-p-anisidine	80.6	[56]
N-(4-N,N-dimethylaminobenzal)-p-toluidine	79.1	[57]
N-(4-N,N-dimethylaminobenzal)-2,4-dinitroaniline	75.9	[57]
Resorcinol derivative DIH	86.2	This work

### 3.11. Explanation of molecular docking data

The investigated 4,6-dihydroxyisophthalohydrazide type inhibitor (DIH), was chosen for molecular docking experiments to emphasize their mode of action. It docked with binding energies of -83.2 KJ/mol, compared to -76.2 KJ/mol for the substrate, which is a good value indicating increased binding affinities. The crucial amino acids, Arg 201 and Ala 299 created strong binding connections. It had two binding affinity interactions, one as an HB-donor and the other as an HB-acceptor, as shown in Figure 12.

### 3.12. Mechanism of action

Electrostatic interaction between the inhibitor molecules and the carbon steel surface through protonated heteroatoms and various linkages determines the adsorption behavior of the resultant protective layer. Benzene-ring electron interactions with Fe atoms' empty d-orbitals and the donor-acceptor interactions of iron (C1018 steel) surfaces with the lone electron were utilized to validate the inhibitor molecule's contact with the

carbon steel surface using two primary adsorption techniques (N and O). These active electrons share the Fe atom's d-orbitals. In Figure 12, you can see an illustration of a proposal.

### 3.13. Comparison between the resorcinol derivative DIH and other inhibitors reported in the literature

The comparison between the investigated DIH compound and other inhibitors reported in the literature for corrosion protection of steel at the same experimental conditions are summarized in Table 12. This comparison shows that the DIH compound is more effective as a corrosion inhibitor than other inhibitors.

## 4. Conclusions

DIH, a resorcinol derivative, is synthesized and its structure is confirmed by <sup>1</sup>HNMR. DIH is examined as a corrosion inhibitor for CS in 0.5 mole L<sup>-1</sup> HCl. The mitigation efficacy of DIH improved as its concentration is increased in corrosive media. On the other hand, the efficacy decreased with rising temperature. DIH compound is a mixed-type inhibitor. The inhibition action of the DIH compound is governed by charge transfer. The adsorption of the DIH compound followed Langmuir isotherm. SEM and AFM results indicated the formation of a compact layer of the DIH compound at CS. The quantum properties confirmed that the inhibitor has high inhibitory effectiveness. The DIH compound inhibited the growth of SRB bacteria.

## References

- [1] A. Singh, I. Ahamad, V. K. Singh, M. A. Quraishi, Inhibition Effect of Environmentally Benign Karanj (*Pongamia pinnata*) Seed Extract on Corrosion of Mild Steel in Hydrochloric Acid Solution, *Journal of Solid State Electrochemistry* 15 (2011) 1087–1097.
- [2] E. Gutierrez, J. A. Rodriguez, J. Cruz-Borbolla, J. G. A. Rodriguez, P. Thangarasu, Development of a predictive model for corrosion inhibition of carbon steel by imidazole and benzimidazole derivatives, *Corros. Sci* 108 (2016) 23–35.
- [3] G. Schmitt, Application of Inhibitors for Acid Media: Report prepared for the European Federation of Corrosion Working Party on Inhibitors, *Br. Corros. J* 19 (1984) 165–176.

- [4] U. Leon-Silva, M. Nicho, J. Gonzalez-Rodriguez, J. Nava, V. Salinas-Bravo, Effect of thermal annealing on the corrosion protection of stainless steel by poly (3-octyl thiophene), *J. Solid State Electrochem* 14 (2010) 1086–1092.
- [5] V. N. Banu, S. S. S. Kumaran, Investigation of the inhibitive effect of Tween 20 self-assembling nanofilms on corrosion of carbon steel, *J. Alloys Compd* 675 (2016) 139–148.
- [6] M. Bouklah, B. Hammouti, A. Aouniti, T. Benhadda, Thiophene derivatives as effective inhibitors for the corrosion of steel in 0.5 M H<sub>2</sub>SO<sub>4</sub> 49 (2004) 225–228.
- [7] A. Popova, M. Christov, S. Raichev, E. Sokolova, Adsorption and Inhibitive Properties of Benzimidazole Derivatives in Acid Mild Steel Corrosion, *Corros. Sci* 46 (2004) 1333–1350.
- [8] L. M. Vracar, D. M. Drazi, Adsorption and corrosion inhibitive properties of some organic molecules on an iron electrode in sulfuric acid, *Corros. Sci* 44 (2002) 166–170.
- [9] R. Farahmand, B. Sohrabi, A. Gha, Synergistic effect of molybdenum coating and SDS surfactant on corrosion inhibition of mild steel in presence of 3.5 % NaCl, *Corrosion Science* 136 (2018) 393–401.
- [10] M, Synergistic corrosion protection for galvanized steel in 3.0% NaCl solution by sodium gluconate and cationic surfactant, *Journal of Molecular Liquids* 220 (2016) 549–557.
- [11] S. Javadian, A. Yousefi, J. Neshati, Synergistic effect of mixed cationic and anionic surfactants on the corrosion inhibitor behavior of mild steel in 3.5% NaCl, *Applied Surface Science* 285 (2013) 674–681.
- [12] Y. Peng, A. E. Hughes, G. B. Deacon, C. Junk, B. R. W. Hinton, M. Forsyth, A. E. A. Somers, study of rare-earth 3-(4-methylbenzoyl)-propanoate compounds as corrosion inhibitors for AS1020 mild steel in NaCl solutions, *Corrosion Science* 145 (2018) 199–211.
- [13] D. N. Nam, H. P. Van, N. T. Hoai, V. T. T. Thu, A study on the mixed corrosion inhibitor with a dominant cathodic inhibitor for mild steel in aqueous chloride solution, *Journal of the Taiwan Institute of Chemical Engineers* 91 (2018) 556–569.
- [14] M. Finsgara, B. Petovar, K. Khanari, The corrosion inhibition of certain azoles on steel in chloride media: Electrochemistry and surface analysis, *Corrosion Science* 111 (2016) 370–381.
- [15] H. S. Lee, H. M. Yang, J. K. Singh, S. K. Prasad, Corrosion mitigation of steel rebars in chloride contaminated concrete pore solution using inhibitor: An electrochemical investigation, *Construction and Building Materials* 173 (2018) 443–451.
- [16] Z. Mirzakhazadeh, A. Kosari, M. H. Moayed, R. Naderi, P. Taheri, J. M. C. Mol, Enhanced corrosion protection of mild steel by the synergetic effect of zinc aluminum polyphosphate and 2-mercaptobenzimidazole inhibitors incorporated in epoxy polyamide coatings, *Corrosion Science* 138 (6) (2018) 372–379.
- [17] H. Tian, W. Li, A. Liu, X. Gao, P. Han, R. Ding, Yang, Controlled delivery of multi-substituted triazole by metal-organic framework for efficient inhibition of mild steel corrosion in neutral chloride solution, *Corrosion Science* 131 (2018) 1–16.
- [18] N. N. Taheri, B. Ramezanzadeh, M. Mahdavian, In-situ synthesis of Zn doped polyaniline on graphene oxide for inhibition of mild steel corrosion in 3.5 wt. % chloride solution, *Journal of Industrial and Engineering Chemistry* 63 (2018) 322–339.
- [19] Y. Zhou, B. Zuo, Lin, The compounded inhibition of sodium molybdate and benzotriazole on pitting corrosion of Q235 steel in NaCl NaHCO<sub>3</sub> solution, *Materials Chemistry and Physics* 192 (2017) 86–93.
- [20] M. Mobin, R. Aslam, Experimental and theoretical study on corrosion inhibition performance of environmentally benign non-ionic surfactants for mild steel in 3.5 % NaCl solution, *Process Safety and Environmental Protection* 114 (2013) 279–295.
- [21] A. Al-Sabagh, N. E. Basiony, S. Sadeek, M. Migahed (2018).
- [22] M. Behpour, S. Ghoreishi, N. Mohammadi, N. Soltani, M. Salavati-Niasari, Investigation of some Schiff base compounds containing disulfide bond as HCl corrosion inhibitors for mild steel, *Corros. Sci* 52 (2010) 4046–4057.
- [23] A. Samide, I. Bibicu, Kinetics corrosion process of carbon steel in hydrochloric acid in absence and presence of 2- (cyclohexylaminomercapto) benzothiazole, *Surf. Interface Anal* 40 (2008) 944–952.
- [24] R. Solmaz, Investigation of the inhibition effect of 5-((E)-4-phenylbuta-1, 3-dienylideneamino)-1, 3, 4-thiadiazole-2-thiol Schiff base on mild steel corrosion in hydrochloric acid, *Corros. Sci* 52 (2010) 3321–3330.
- [25] H. E. Sayed, S. Elsayedd, H. Ashour, E. Zak, H. E. Nagy, Novel acrylamide ionic liquids as anti-corrosion for X-65 steel dissolution in acid medium: Adsorption, hydrogen evolution and mechanism, *J. Mol. Struct* 1168 (2018) 106–114.
- [26] M. C. Li, L. L. Jiang, W. Q. Zhang, Y. H. Qian, S. Z. Luo, J. N. Shen, Electrochemical corrosion behavior of nanocrystalline zinc coatings in 3.5% NaCl solutions, *J. Solid State Electrochem* 11 (2007) 1319–1325.
- [27] F. Walsh, S. Amyes, Microbiology and drug resistance mechanisms of fully resistant pathogens, *Curr. Opin. Microbiol* 7 (2004) 439–439.
- [28] M. S. Nafie, M. A. Tantawy, G. A. Elmgeed, Screening of different drug design tools to predict the mode of action of steroidal derivatives as anti-cancer agents, *Steroids* 152 (2019) 108–485.
- [29] A. S. Fouda, S. M. Rashwan, M. M. Kamel, E. A. Haleem, Juglans Regia Extract (JRE) as Eco-Friendly Inhibitor for Aluminum Metal in Hydrochloric Acid Medium, *Biointerface Research in Applied Chemistry* 10 (5) (2020) 6398–6416.
- [30] International Organization for Standardization (25178) for 3D surface texture parameters.

- [31] American S. T. M., Designation (4412-84).
- [32] N. Perez, *Electrochemistry and Corrosion Science*. First Edition Part 1 (2016) 1–23.
- [33] H. M. A. El-Lateef, V. Abbasov, L. Aliyeva, E. Qasimov, I. Ismayilov, Applicability of Novel Anionic Surfactant as a Corrosion Inhibitor of Mild Steel and for Removing Thin Petroleum Films from Water Surface Mater, *Chem. Phys* (142) (2013).
- [34] L. H. Abdel-Rahman, A. M. Abu-Dief, M. A.-E. Sayed, M. M. Zikry, Nano Sized Moringa oleifera an Effective Strategy for Pb(II) ions Removal from Aqueous Solution, *J. Chem. Mater. Res* 8 (2016) 8–22.
- [35] L. Abdel-Rahman, B. Al-Farhan, A. Abu-Dief, M. Zikry, Removal of Toxic Pb(II) Ions from Aqueous Solution by Nano-Sized Flamboyant Pod (*Delonix regia*), *Archives in Chemical Research* 1 (2016) 1–3.
- [36] M. Schorr, J. Yahalom, The significance of the energy of activation for the dissolution reaction of metal in acids, *Corrosion Science* 12 (1972) 867–868.
- [37] H. Fan, S. Li, Z. Zhao, H. Wang, Z. Shi, L. Zhang, Inhibition of brass corrosion in sodium chloride solutions by self-assembled silane films, *Corros. Sci* 53 (2011) 4273–4281.
- [38] A. Singh, S. Mohapatra, B. Pani, the Corrosion inhibition effect of Aloe Vera gel: Gravimetric and electrochemical study, *J. Ind. Eng. Chem* 33 (2016) 288–297.
- [39] M. Elachouri, M. S. Hajji, M. Salem, S. Kertit, J. Aride, R. Coudert, E. Essassi, Some Nonionic Surfactants as Inhibitors of the Corrosion of Iron in Acid Chloride Solutions, *Corrosion* 52 (1996) 103–103.
- [40] F. Bentiss, M. Lebrini, M. Lagrenée, Thermodynamic characterization of metal dissolution and inhibitor adsorption processes in mild steel/2,5-bis(n-thienyl)-1,3,4-thiadiazoles/hydrochloric acid system, *Corrosion Science* 47 (12) (2005) 2915–2931.
- [41] I. Langmuir, the constitution and fundamental properties of solids and liquids. Part I. Solids, *J. Am. Chem. Soc* 38 (11) (1916) 2221–2295.
- [42] A. L. Essaghoulani, H. Elmsellem, M. Boulhaoua, M. Ellouz, M. E. Hafii, N. K. Sebbar, E. M. Essassi, M. Bouabdellaoui, A. Aouniti, B. Hammouti, Adsorption proprieties and inhibition of mild steel corrosion in HCl solution by 1-Benzyl-4-phenyl-2,3-dihydro-1H-1,5-benzodiazepine-2-one, *Der Pharma Chemica* 8 (2) (2016) 347–355.
- [43] A. K. Singh, M. A. Quraishi, Investigation of the effect of disulfiram on corrosion of mild steel in hydrochloric acid solution, *Corrosion Science* 53 (4) (2011) 1288–1297.
- [44] S. Issaadi, T. Douadi, A. Zouaoui, S. Chafaa, M. A. Khan, G. Bouet, Novel thiophene symmetrical Schiff base compounds as corrosion inhibitor for mild steel in acidic media, *Corrosion Science* 53 (4) (2011) 1484–1488.
- [45] M. M. Kamel, A. A. S. Fouda, S. M. Rashwan, O. Abdelkader, Paprika extract: a green inhibitor for mitigating carbon steel disintegration in 1 M HCl pickling solution, *Green Chemistry Letters and Reviews* 14 (4) (2021) 598–609.
- [46] M. A. Hegazy, S. M. Rashwan, S. Melek, M. M. Kamel, Synthesis, characterization and mitigation action of innovative Schiff base on steel disintegration in sulfuric acid solution, *Materials Chemistry and Physics* 267 (2021).
- [47] A. Lalitha, S. Ramesh, S. Rajeswari, Surface protection of copper in acid medium by azoles and surfactants, *Electrochimica Acta* 51 (1) (2005) 47–55.
- [48] D. Zhang, L. Gao, G. Zhou, Inhibition of copper corrosion in aerated hydrochloric acid solution by heterocyclic compounds containing a mercapto group, *Corrosion Science* 46 (12) (2004) 3031–3040.
- [49] N. A. Negm, M. A. Migahed, R. K. Farag, A. A. Fadda, M. K. Awad, M. M. Shaban, High performance corrosion inhibition of novel tricationic surfactants on carbon steel in formation water: Electrochemical and computational evaluations, *Journal of Molecular Liquids* 262 (2018) 363–375.
- [50] S. Martinez, Inhibitory mechanism of mimosa tannin using molecular modeling and substitutional adsorption isotherms, *Mater. Chem. Phys* 77 (2003) 569–576.
- [51] B. Xu, Experimental and theoretical evaluation of two pyridinecarboxaldehyde thiosemicarbazone compounds as corrosion inhibitors for mild steel in hydrochloric acid solution, *Corros Sci* 78 (2014) 260–268.
- [52] F. Caleyó, Probability distribution of pitting corrosion depth and rate in underground pipelines: a Monte Carlo study, *Corros Sci* 51 (9) (2009) 1925–1934.
- [53] P. Ammal, M. Prajila, A. Joseph, Effect of substitution and temperature on the corrosion inhibition properties of benzimidazole bearing 1, 3, 4-oxadiazoles for mild steel in sulphuric acid: physicochemical and theoretical studies, *J Environ Chem Eng* 6 (1) (2018) 1072–1085.
- [54] O. U. Abakedi, V. N. Mkpenie, E. G. Ukpong, Anti-corrosion behaviour of 4( p -tolylidiazonyl)-2-(( E )- ( p -tolylimino)methyl) phenol on mild steel in 1M H<sub>2</sub>SO<sub>4</sub>: Experimental and theoretical studies, *Scientific African* 7 (2020).
- [55] D. Mahalakshmi, V. Hemapriya, E. P. Subramaniam, S. Chitra, Synergistic effect of antibiotics on the inhibition property of aminothiazolyl coumarin for corrosion of mild steel in 0.5 M H<sub>2</sub>SO<sub>4</sub>, *J. Mol. Liq* 284 (2019) 316–327.
- [56] Evaluating synthesized Schiff base as corrosion inhibitor on carbon steel in 0.5 M HCl and 0.5 M H<sub>2</sub>SO<sub>4</sub> 4 (2016) 21–35.
- [57] T. Sethi, A. Chaturvedi, R. K. Upadhyay, S. P. Mathur, corrosion inhibitory effects of some Schiff's bases on mild steel in acid media, *J. Chil. Chem. Soc* 52 (2007) 1206–1213.